Research on Stability Control and Optimal Algorithm of Regeneration for Distributed Drive Four-wheel Drive Vehicles

YUEHANG DONG, YUANYUAN YANG, HONGJUN ZHAI, CHANGMING ZHAO
Ningbo Geely Automobile Research and Development Co., Ltd,
No. 918 Binhai 4th Rd, Hangzhou Bay New District, Ningbo, Zhejiang
CHINA

Abstract: - For the braking regeneration process of distributed 4WD vehicles, based on the requirements of ECE R13 regulations and I curve and on the premise of vehicle stability, further consider achieving the optimal braking energy feedback. On the distributed drive control, a fuzzy control algorithm does design to combine stability control with optimal regenerative braking energy feedback control, and the limiting conditions of battery and motor on torque output are comprehensively considered. The driving or braking torque demand of a four-wheel drive motor is given, which improves the stability of a four-wheel drive vehicle and achieves optimal braking energy recovery. Finally, the effectiveness of the strategy is verified by the actual vehicle tests under pylon course slalom and double-shift conditions.

Key-Words: - distributed drive, four-wheel drive, regenerative braking, yaw velocity, side slip angle, handling stability, I curve, ECE R13 regulation

Received: July 24, 2022. Revised: April 19, 2023. Accepted: May 25, 2023. Published: July 6, 2023.

1 Preface

The distributed drive has become the leading research direction for most automakers. Since all four wheels of distributed drive 4WD vehicles are involved in driving, there are many types of research on stability control of 4WD vehicles based on yaw rate and centroid sideslip angle control during the driving process, while there are few kinds of research on brake process stability control and optimal brake energy feedback. There needs to be more discussion, especially for the combination of optimal braking energy feedback and anti-slip braking during the braking process, which meets the requirements of ECE R13 regulations. This article discusses the control strategy and calculation formula for calculating the optimal braking feedback of distributed four-wheel drive vehicles equipped with four motors during braking, which meets the requirements of ECE R13 regulations and is verified through actual vehicle tests. Research on Parallel Braking Control of Distributed Four-wheel-drive

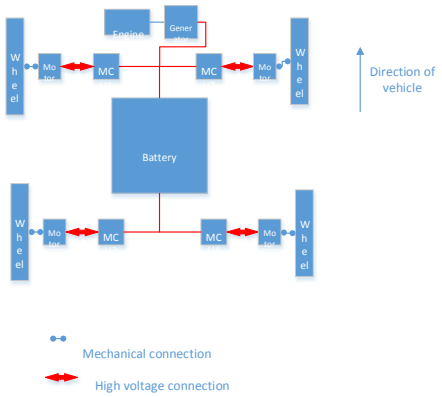

Fig. 1: Power system layout of 4WD pure electric vehicles

Electric Vehicle, [1], studied the influence of vehicle speed constraints on the final four-wheel torque output based on fuzzy control and considering battery SOC; however, the ECE R13 restriction and optimal braking feedback were not considered. Taking a two-axle four-wheel drive electric vehicle as the research object, a recent study developed the braking energy recovery strategy, [2], based on the

I-curve braking force distribution; this literature is only based on simulation research and does not have actual vehicle testing to verify the effectiveness of the strategy. Literature, [3], takes the two-axle four-wheel drive electric vehicle as the research object and develops the braking energy recovery strategy, [3], based on the I-curve braking force distribution. The description of braking strategy after ESP needs to be described, and the vehicle speed prediction strategy in literature, [3], is not defined. Literature, [4], describes driver intention identification based on the brake pedal, [4], only simulation analysis was conducted without actual vehicle test validation, and there was no description of the speed prediction algorithm. A recent study analyzed yaw control based on front and rear loads, [5]. Still, there is no analysis of vehicle speed prediction and acceleration changes, there aren't prediction algorithms for future velocity and acceleration, and there aren't control algorithms for vehicle stability control. In this paper, based on the comprehensive consideration of the braking process and the vehicle stability control, the slip rate, motor fault state constraints, and front and rear load constraints, the optimal feedback braking function is formulated, and the practicability of the control strategy is verified through the actual vehicle test. The layout of four-wheel drive and two-drive vehicles is shown in Figure 1 and Figure 2. The motors can be wheel-side motors, hub motors, and ordinary motors.

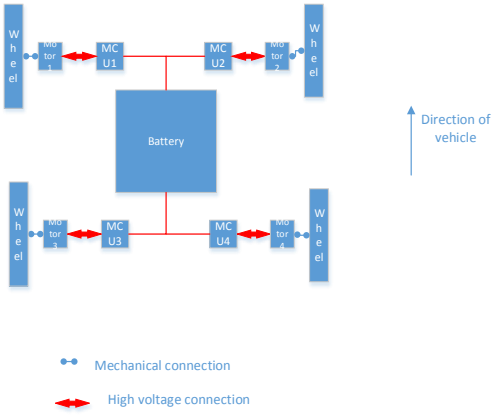

Fig. 2: Four-wheel drive power system layout of REEV

In Figure 1 and Figure 2, MCU1: motor controller 1

MCU2: motor controller 2

MCU3: motor controller 3

MCU4 : Motor controller 4

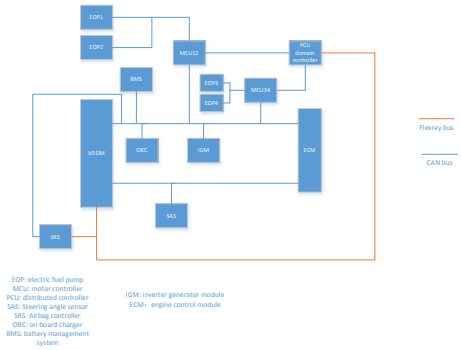

Fig. 3: Topology of the main controller of distributed drive

EOP1 is responsible for the cooling of motor controller 1 and motor 1, EOP2 is responsible for the cooling of motor controller 2 and motor 2, EOP3 is responsible for the cooling of motor controller 3 and motor 3, and EOP4 is responsible for the cooling of motor controller 4 and motor 4. MCU 12 receives the control command sent by PCU to control motors 1 and 2, and MCU 34 receives the control command sent by PCU to control motors 3 and 4. The ECM receives the PCU command to start the engine and drive the generator to generate electricity for the drive motor and high-voltage battery. The IGM controls the generator to generate electricity. BMS controls battery charging and discharging. VDDM is the chassis domain controller responsible for ABS, ESP, TCS, VDC, and other functions. SRS is responsible for safety belt and collision safety. SAS sends steering wheel angle information to PCU for yaw rate control. The topology of the main controller of the distributed drive is presented in Figure 3.

2 Stability Control and Optimal Braking Feedback Control Strategy

2.1 Stability Control and Optimal Regenerative Feedback

Develop a Figure 4 (appendix) strategy based on stability control and optimal feedback.

This section discusses achieving the optimal control strategy for braking feedback energy during the braking process. After determining that the brake pedal is pressed, enter the braking process and follow the optimal energy feedback control curve O-A-B-C-D-E-F, which is set in Figure 10. During the braking process, estimate the ideal yaw rate and the required center of mass sideslip angle, [6], [7], collect the actual yaw rate, [8], and calculate the current center of mass sideslip angle. Then, based on the difference between the ideal yaw rate and the actual yaw rate, the estimated center of mass sideslip angle and the calculated current center of mass sideslip angle are used as inputs. The fuzzy control strategy, which is described in section 2.2, is adopted, and the effect of ESP/ABS interference is considered, Output the torque requirements of four motors, control the four wheels, and achieve control of vehicle stability, thereby achieving the dual goals of optimal braking feedback energy and vehicle stability control, [9], [10].

2.2 Determination of Vehicle Stable Yaw Moment based on Fuzzy Control Theory

Based on the fuzzy control theory, [11], the fuzzy controller of the expected yaw moment, [12], is designed, as shown in Figure 5.

The controller input variable is the desired yaw rate ω_d and actual yaw rate ω difference e_ω and the desired centroid sideslip angle β_d and actually estimated centroid side slip angle β difference e_β ; the controller output variable is the expected yaw moment M_{zd}。

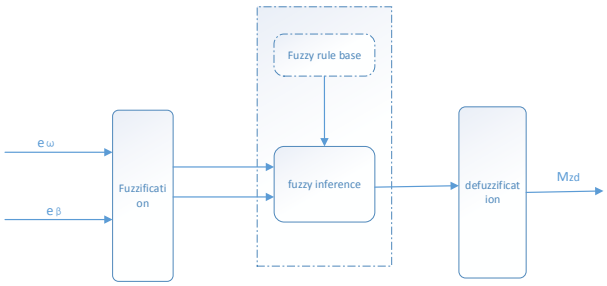

Fig. 5: Fuzzy controller of expected yaw moment

1) Fuzzification: First, the precise input value will be fuzzed into fuzzy values. The input variable e_ω and e_β will be equally divided into 5 fuzzy sets, and the output variable M_{zd} is divided into seven fuzzy sets, see Table 1 for details. Establish yaw rate error e_ω Membership function, centroid sideslip error e_β Membership function, expected yaw moment M_{zd} membership function, as shown in Figure 6, Figure 7 and Figure 8.

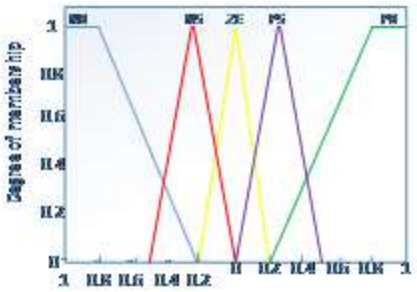

Fig. 6: Yaw rate error membership function

Table 1. Input and output fuzzy set of expected yaw moment controller

NB（Negative bigness）	NB （Negative bigness）	NB （Negative bigness）
NS（Negative small）	NS （Negative small）	NM（Negative middle）
ZE （Zero）	ZE （Zero）	NS（Negative small）
PS （Positive small）	PS （Positive small）	ZE （Zero）
PB （Positive bigness）	PB （Positive bigness）	PS （Positive small）
——	——	PM (Positive middle)
——	——	PB （Positive bigness）

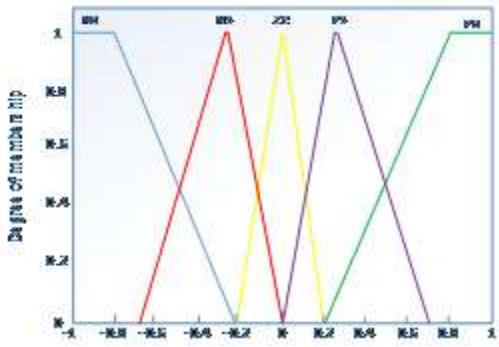

Fig. 7: Membership function of centroid sideslip angle error

2) Fuzzy reasoning:

fuzzy reasoning is the core of fuzzy controller, that is to use fuzzy language to describe the logical relationship between input and output variables after fuzzing, see Table 2 for details.

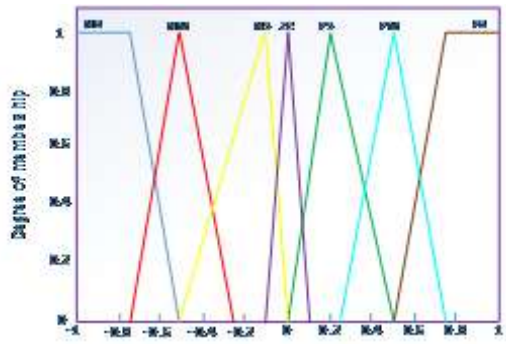

Fig. 8: Desired yaw moment M_{zd} membership function

3) defuzzification:

After obtaining the fuzzy value of the output value, it is necessary to convert the fuzzy value into an accurate value through ambiguity resolution before it can be used for subsequent control.

2.3 Develop a Seven-Degree-Of-Freedom Vehicle Model, Distribute the Yaw Moment to the Four Wheels according to the Front and Rear Axle Load Ratio

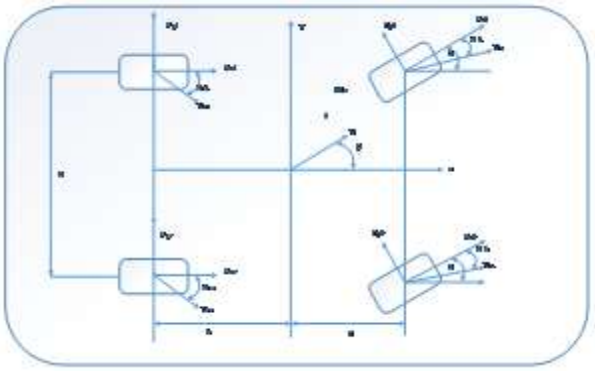

Fig. 9: Simplified diagram of 7-DOF vehicle model

1 :Develop the vehicle 7-degree of freedom model, as shown in Figure 9,

where d (m) is the track width, $F_{yrl}(m)$ is the driving force of the left wheel of the rear axle in the Y-axis direction, $F_{xrl}(m)$ is the driving force in the X-axis direction of the left wheel of the rear axle, F_{yrr}(m) is the driving force of the right wheel of the rear axle in the Y-axis direction, F_{xrr}(m)is the driving

force of the right wheel of the rear axle in the X-axis direction.

Table 2. Fuzzy rule reasoning of desired yaw moment controller

	e_β(NB)	e_β(NS)	e_β(ZO)	e_β(PS)	e_β(PB)
e_ω(NB)	NB	NB	NB	NM	NM
e_ω(NS)	NB	NM	NM	NS	NS
e_ω(ZO)	NS	NS	ZO	PS	PS
e_ω(PS)	PS	PS	PM	PM	PB
e_ω(PB)	PM	PM	PB	PB	PB

F_{yfl}(m) is the driving force of the left wheel of the front axle in the Y- axis direction, F_{xfr}(m) is the driving force of the left wheel of the front axle in the X-axis direction, F_{yfr}(m) is the driving force in the Y-axis direction of the right wheel of the front axle, F_{xfr}(m) is the driving force in the X-axis direction of the right wheel of the front axle. l_r(m) is the distance from the rear axle to the vehicle centroid, l_f(m) is the distance from the front axle to the vehicle centroid, ɣ (rad/s) is the yaw rate, β (rad) is the sideslip angle of the vehicle centroid.

2：Distribute the yaw moment to the four wheels according to the front and rear axle load ratio.

According to the 7-DOF vehicle model, considering the longitudinal force and the Y-axis moment generated by the longitudinal force, the following formula is obtained:

$$\Delta \mathrm{M}_x = l_f\left(F_{xfl} - F_{xrl}\right)\sin\delta + \frac{d}{2}\left[\left(F_{xfr} - F_{xfl}\right)\cos\delta + \frac{d}{2}\left(F_{xrr} - F_{xrl}\right)\right] \quad (1)$$

Because the steering angle is small during steering, so $\cos\delta \approx 1$, $\sin\delta \approx 0$. So formula (1) can be converted into：

$$\Delta \mathrm{M}_x = \frac{d}{2}\left[\left(F_{xfr} - F_{xfl}\right) + \left(F_{xrr} - F_{xrl}\right)\right] \quad (2)$$

$$M_{zd} = M_f + M_r \quad (3)$$

Where M_{zd} is the stable yaw moment calculated in Figure 5 based on the centroid sideslip angle and yaw rate, M_f is the front axle yaw moment, M_r is the rear axle yaw moment.

According to the front and rear load of the vehicle, the distribution is as follows:

$$M_f = k_f M_{zd} = \frac{F_{zfl}+F_{zfr}}{F_{zfl}+F_{zfr}+F_{zrl}+F_{zrr}} M_{zd} \quad (4)$$

$$M_r = k_r M_{zd} = \frac{F_{zrr}+F_{zrl}}{F_{zfl}+F_{zfr}+F_{zrl}+F_{zrr}} M_{zd} \quad (5)$$

$$\left|T_{fl}\right| = \left|T_{fr}\right| \ ,\left|T_{rl}\right| = \left|T_{rr}\right| \quad (6)$$

Where F_{zfl} is the vertical load of the left wheel of the front axle, F_{zfr} is the front axle right wheel vertical load, F_{zrl} is a vertical load of the left wheel of the rear axle, F_{zrr} is rear axle right wheel vertical load. k_f is the front wheel cornering stiffness, k_r is the rear wheel cornering stiffness T_{fl} is the torque of the left wheel of the front axle, T_{fr} is the torque of the right wheel of the front axle, T_{rl} is the torque of the left wheel of the rear axle, T_{rr} is the torque of the right wheel of the rear axle.

The relationship between motor torque and longitudinal driving force is:

$$F_x = \frac{T_m}{R} \quad (7)$$

T_m（Nm）is the motor torque. Combining the formula (2) and (7), formula (8) can be obtained:

$$M_{zd} = \frac{d}{2\mathrm{R}}\left[\left(T_{fr} - T_{fl}\right) + \left(T_{rr} - T_{rl}\right)\right] \quad (8)$$

Combining equations (4), (5) and (6), the torque value of yaw torque based on load proportion at four wheels is：

$$T_{fl} = -k_f \frac{M_{zd}R}{d} \quad (9)$$

$$T_{fr} = k_f \frac{M_{zd}R}{d} \quad (10)$$

$$T_{rl} = -k_r \frac{M_{zd}R}{d} \quad (11)$$

$$T_{rr} = k_r \frac{M_{zd}R}{d} \quad (12)$$

2.4 Calculate the Braking Torque Demand of Four Wheels according to the Front and Rear Loads

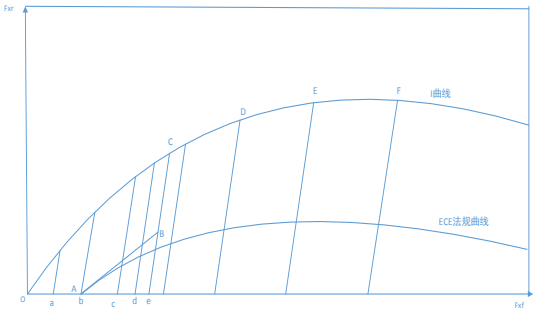

Fig. 10: Optimal braking torque distribution of each wheel based on ECE R13 regulation and braking force I curve

The abscissa is the front axle braking force, and the ordinate is the rear axle braking force. F stands for the front, and r stands for real. Fx represents the braking force function.

Instruction：

1：The straight line AB is the tangent of the ECE regulation curve after the extension of point A, and point A is the intersection point of the ECE regulation curve at F_{xf} axis. Point B is the intersection point of the vertical line at the maximum braking force of the two motors on the front axle and the tangent line AB and then extends to the I curve along section BC of the f line group (f line group is the relationship curve of the front and rear ground brake force when the rear wheels are not locked and the front wheels are locked on the roads with different road adhesion coefficients), and point C is the intersection point of the braking force f line group extending to the I curve and the I curve.

I curve formula is：

$$F_{br} = \frac{1}{2}\left[\frac{G}{h_g}\sqrt{b^2 + \frac{4h_gL}{G}F_{bf}} - \left(\frac{Gb}{h_g} + 2F_{bf}\right)\right] \quad (13)$$

Among:

F_{br}（N） is the total braking force of the rear axle brake; F_{bf}(N) is the total braking force of the front axle brake; G(N) is the vehicle gravity, b(m) is the distance from the vehicle centroid to the rear axle; L(m) is the wheelbase; h_g(m) is the distance from the vehicle centroid to the ground;

2: The OA segment function is:

$$F_{bf} = zG \quad (14)$$

$$F_{br} = 0 \quad (15)$$

Where z is the braking intensity.

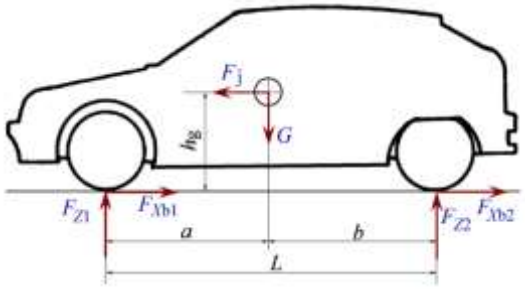

Fig. 11: Force diagram of vehicle braking

According to Figure 11, the moment of force at the earth connection point in the rear wheel can be obtained:

$$F_{z1}L = Gb + m\frac{du}{dt}h_g \quad (16)$$

Where: F_{z1}(N) is the normal reaction force of the ground to the front axle, G(N) is the vehicle gravity, and b(m) is the distance from the rear axle centerline to the center of mass. h_g(m) is the height of the vehicle centroid, $\frac{du}{dt}\left(m/s^2\right)$ is the vehicle deceleration. Calculate the moment of force at the earth connection point in the front wheel,

$$F_{z2}L = Ga - m\frac{du}{dt}h_g \quad (17)$$

Where, F_{z2} (N) is the normal reaction force of the ground to the rear axle, an (m) is the distance from the center line of the front axle to the center of mass,

order

$$\frac{du}{dt} = \mathrm{Zg} \tag{18}$$

Z is the braking strength, and g is the acceleration of gravity.

3: Then the CF segment function can also be expressed as:

$$F_{bf} = \frac{zG(b+zh_g)}{L} \tag{19}$$

$$F_{br} = \frac{zG(a-zh_g)}{L} \tag{20}$$

4: ECE curve formula is：

$$F_{bf} = \frac{z+0.04}{0.85} \times \frac{G(b+zh_g)}{L} \tag{21}$$

（0.2<z<0.8）

$$F_{br} = zG - F_{bf} \tag{22}$$

5: BC straight line formula is：

$$F_{br} = \frac{L-\emptyset h_g}{\emptyset h_g} \times F_{bf} - \frac{Gb}{h_g} \tag{23}$$

In Formula (23), $\emptyset$ is the road adhesion coefficient. The coordinate of point A is $(F_{fA}, 0)$, F_{fA} is the intersection point of the ECE curve and F_{xf} axis.

6: The straight line formula of the AB section is：The AB linear equation is:

$$F_{br} = \frac{0.85a - h_g\left(\frac{1.7\times F_{fA}}{G}+0.034\right)}{(F_{fA}\times 0.85+0.034+\frac{0.85\times F_{fA}}{G})h_g+0.85b}(F_{bf} - F_{fA}) \tag{24}$$

Moreover, it is noticed that Figure 12 presents the flow chart of braking anti-skid strategy. In the (24) formula, an (m) is the distance from the front axle centerline to the vehicle centroid.

7:

1) When the total braking force demand of the vehicle is in the OA section, the braking force is entirely provided by the feedback braking torque of the two motors of the front axle.

2) When the total braking force demand of the vehicle is in section AB, the braking force of the front axle is still provided by the feedback braking torque of the two motors of the front axle. If the braking force demand of the rear axle is less than the sum of the feedback braking torque of the two motors of the rear axle, the braking force of the rear axle is provided by the two motors of the rear axle. If the braking force demand of the rear axle is greater than the feedback braking force that can be provided by the two motors of the rear axle, the braking force is first provided by the feedback braking force of the two motors of the rear axle, and the remaining insufficient parts are supplemented by hydraulic pressing power.

3) When the total braking force demand of the vehicle is in the BC, CD, DE, and EF sections, the front axle braking force is still preferentially provided by the feedback braking force of the two motors of the front axle. The insufficient part is supplemented by the hydraulic braking force of the front axle, the rear axle is preferentially provided by the feedback braking force of the two motors of the rear axle, and the insufficient part is supplemented by the hydraulic braking force of the rear axle.

4) After z>0.7, the front and rear axle braking forces are all provided by hydraulic braking force, and the electric braking is quit.

8：If the yaw angle measured by the center of mass or the yaw rate exceeds the threshold value, and the yaw control is involved, add the yaw moment to each wheel (the yaw moment value is from formula (9) to (12)), and combine the front and rear axle braking force F_{bf} and F_{br}, the braking torque is calculated as follows:

$$\begin{cases} M_{bfl+M} = \dfrac{R \times F_{bf}}{2} - \boldsymbol{k_f}\dfrac{\boldsymbol{M_{zd}R}}{\boldsymbol{d}} \ (\mathbf{25}) \\ M_{bfr+M} = \dfrac{R \times F_{bf}}{2} + \boldsymbol{k_f}\dfrac{\boldsymbol{M_{zd}R}}{\boldsymbol{d}} \ (\mathbf{26}) \\ M_{brl+M} = \dfrac{R \times F_{br}}{2} - \boldsymbol{k_r}\dfrac{\boldsymbol{M_{zd}R}}{\boldsymbol{d}} \ (\mathbf{27}) \\ M_{brr+M} = \dfrac{R \times F_{br}}{2} + \boldsymbol{k_r}\dfrac{\boldsymbol{M_{zd}R}}{\boldsymbol{d}} \ (\mathbf{28}) \end{cases}$$

Where M_{bfl+M} is the braking torque of the front left wheel after the stability yaw moment intervention, M_{bfr+M} is the braking torque of the front right wheel after the stability yaw moment intervention, M_{brl+M} is the braking torque of the left wheel after the stability yaw moment is involved, M_{brr+M} is the braking torque of the rear right wheel after the stability yaw moment is involved.

9 : Driving force limit, corresponding to the driving force limit layer in Figure 4:
1): If the motor fails, the motor controller will limit the torque, limit the power and close the tube according to the detailed fault level.
2): The total power of the four motors cannot exceed the maximum charging and discharging power limit provided by the battery. $\sum_{i=1}^{4} P_i \leq P_{bat\_max}$, where P_i is the motor power, P_{bat_max} is the maximum charge and discharge power of the battery.
3) The driving or charging torque of a single motor cannot exceed the limit value given by each motor controller. $T_{req} \leq T_{mot_{availble}}$, where T_{req} is the motor torque demand sent by the vehicle controller to each motor controller, $T_{mot\_\max\_availble}$ is the maximum torque each motor can output, which is sent by the controller.
4): Each wheel's driving or braking force shall meet the requirement of making the wheel slip rate s ≤ 20%.
5): The whole vehicle controller judges and outputs the maximum driving force or braking force that each driving wheel motor can provide according to the fault level of the entire vehicle.

2.5 Braking Anti-Skid Control Strategy

See flow chart 12 of braking anti-skid control (see Appendix). In this section, the anti-slip control algorithm is described.
1) First, whether the brake pedal is pressed is judged. If the brake pedal is pressed, the program enters the braking process. Firstly, determine whether the ESP is activated. If the ESP is activated, the anti-slip program will enter the process of stopping the driving torque, reducing the driving torque to 0 within a specified time according to a specific gradient, and cooperating with the ESP system to complete the braking process while avoiding forward impact of the vehicle.
2) If ESP is not activated and enters the anti-slip braking process, the first step is to calculate the slip rate of each wheel based on the effective vehicle speed, determine which wheel is slipping, and perform torque reduction control on the slipping wheel, [13]. Then based on the acceleration, determine whether the deceleration change rate exceeds the preset value, and if it exceeds the preset value, torque intervention should also be carried out.
3) The genetic algorithm+BP neural network algorithm is used to predict the future velocity and acceleration under different driving conditions and driving habits
4) Based on the predicted vehicle speed, predict the sliding trend of each wheel in the future. If the wheel slip rate exceeds the set value or the deceleration value increases by more than the set value, intervention should be carried out for the braking torque.
5) Determine whether the steering wheel angle exceeds the set value. If it exceeds the set value, the body stability program intervenes, using yaw rate and center of mass sideslip angle as inputs to control the body stability.

6) Based on the above strategy, braking torque will be outputted to four motors and control the braking torque of each wheel.

2.5.1 Longitudinal Speed Calculation

The estimation of longitudinal speed plays a very critical role in vehicle anti-skid control. The estimation of vehicle speed is inaccurate, and the vehicle anti-skid will lose its foundation. According to [14], the estimation method of vehicle speed is shown in Table 3 (see Appendix). Based on the above information, this paper uses a fusion algorithm to calculate the current vehicle speed using the Kalman filter under low-speed conditions. It uses acceleration integral to estimate the current vehicle speed when it is in slip/brake lock conditions. UKF (Unscented Kalman Filter) is used to estimate vehicle speed. UKF is a nonlinear Gaussian filter proposed by JULIER in the 1990s. UKF inherits the basic structure of KF, but UKF does not need to solve the Jacobian matrix but carries out state error propagation based on odorless transformation. Theoretically, the tasteless conversion can approximate the posterior mean and covariance of any nonlinear Gaussian system state with at least third-order Taylor precision. When the nonlinear degree of the target object is improved to a certain level, UKF will have higher accuracy, does not need to linearize the system, and does not need to calculate the Jacobian matrix of the system during the operation process, which can improve the efficiency and stability of the estimation. The state equation of the nonlinear system is as follows：

$$X_k = f(X_{k-1}, U_{k-1}) + W_k \tag{29}$$

Observation equation：

$$Z_k = h(X_{k-1}) + V_k \tag{30}$$

The flow of UKF is described below:

1: initialize

$$\hat{X}_0^a = E(X_0) \tag{31}$$

$$P_0^a = E\left[\left(X_0 - \hat{X}_0^b\right)\left(X_0 - \hat{X}_0^b\right)^T\right] \tag{32}$$

2: Time update section

1） Generate 2n sigma sampling points, which are from the vicinity of the original state and are obtained by proper operation

$$\hat{X}_{k-1}^i = \hat{X}_{k-1}^b + \tilde{X}^{(i)} \tag{33}$$

$$\tilde{X}^{(i)} = \left(\sqrt{nP_{k-1}^b}\right)_i^T \tag{34}$$

$$\tilde{X}^{(n+i)} = -\left(\sqrt{nP_{k-1}^b}\right)_i^T \tag{35}$$

2） Substitute each sampling point into the equation of state to obtain:

$$\hat{X}_k^{(i)} = f(X_{k-1}, U_{k-1}) \tag{36}$$

3） Calculate the mean value of k time：

$$\hat{X}_k^a = \frac{1}{2n}\sum_{i=1}^{2n} \hat{X}_k^{(i)} \tag{37}$$

4） Calculate the covariance at time k

$$P_k^a = \frac{1}{2n}\sum_{i=1}^{2n}(\hat{X}_k^{(i)} - \hat{X}_k^{(a)})(\hat{X}_k^{(i)} - \hat{X}_k^{(a)})^T + Q_{k-1} \tag{38}$$

3: Watch the update section

1） Regenerate a batch of sampling points according to the predicted value

$$\hat{X}_k^{(i)} = \hat{X}_k^a + \tilde{X}^{(i)} \tag{39}$$

$$\tilde{X}^{(i)} = \left(\sqrt{nP_k^a}\right)_i^T \tag{40}$$

$$\tilde{X}^{(n+i)} = -\left(\sqrt{nP_k^a}\right)_i^T \tag{41}$$

2） By substituting each sampling point into the observation equation, we can get:

$$\hat{Z}_k^{(i)} = h(\hat{X}_k^{(i)}) \tag{42}$$

3） Calculate the mean value of time k

$$\hat{Z}_k = \frac{1}{2n}\sum_{i=1}^{2n} \hat{Z}_k^{(i)} \tag{43}$$

4） Calculate the covariance at time k

$$P_Z = \frac{1}{2n}\sum_{i=1}^{2n}\left(\hat{Z}_k^{(i)} - \hat{Z}_k\right)\left(\hat{Z}_k^{(i)} - \hat{Z}_k\right)^T + R_k \tag{44}$$

5） Estimating the covariance between states and observations

$$P_{XZ} = \frac{1}{2n}\sum_{i=1}^{2n}\left(\hat{X}_k^{(i)} - \hat{X}_k^a\right)\left(\hat{Z}_k^{(i)} - \hat{Z}_k\right)^T \tag{45}$$

Finally, the state quantity is updated using Kalman gain:

$$K_k = P_{xz}P_z^{-1} \quad (46)$$

$$\hat{X}_k^b = \hat{X}_k^a + K_k(Z_k - \hat{Z}_k) \quad (47)$$

$$P_k^b = P_k^a - K_k P_z K_k^T \quad (48)$$

Estimated state quantity longitudinal vehicle speed V_x, Lateral speed V_y, Yaw rate ω, longitudinal acceleration A_x, Lateral acceleration A_y .Write as vector

$$X_t = [V_x,\ V_y,\ \omega,\ A_x,\ A_y]^T \quad (49)$$

Observation variable longitudinal acceleration A_x. Lateral accelerationA_y. In the form of a vector,

$$\mathrm{Z(t)} = [A_x, A_y, \omega]^T \quad (50)$$

The equation of state is as follows：

$$V_{x(k)} = V_{x(k-1)} + [A_{x(k-1)} + V_{y(k-1)}\omega_{k-1}]\Delta t \quad (51)$$

$$V_{y(k)} = V_{y(k-1)} + [A_{y(k-1)} - V_{x(k-1)}\omega_{k-1}]\Delta t \quad (52)$$

$$\omega_k = \omega_{k-1} + \frac{M_z}{I_z}\Delta t \quad (53)$$

$$A_{x(k)} = \frac{1}{M} \quad (54)$$

$$\{[F_{x1(k-1)} + F_{x2(k-1)}]\cos\delta - [F_{y1(k-1)} + F_{y2(k-1)}]\sin\delta + F_{x3(k-1)} + F_{x4(k-1)} - F_{w(k-1)} - F_{f(k-1)}\} \quad (55)$$

$$A_{y(k)} = \frac{1}{M}\{[F_{y1(k-1)} + F_{y2(k-1)}] + [F_{x1(k-1)} + F_{x2(k-1)}]\sin\delta + F_{y3(k-1)} + F_{y4(k-1)}\} \quad (56)$$

The observation equation is as follows：

$$\mathrm{Z(t)} = [A_{x(k)}, A_{y(k)}, \omega(k)]^T \quad (57)$$

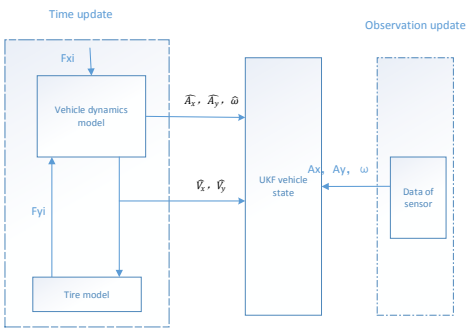

Fig. 13: UKF Vehicle speed estimator estimation process

In addition, Figure 13 presents the UKF Vehicle speed estimator estimation process. When excessive wheel slip/slip occurs, the correlation between wheel speed and vehicle speed decreases rapidly; when the wheels lock or slip completely, the relationship between wheel speed and vehicle speed is no longer relevant. At this time, if the Kalman filter algorithm is still used, the vehicle speed estimation results will have a significant deviation. Therefore, when all wheels have no slip/slip, the vehicle speed Vx is obtained using the wheel speed signal without excessive slip/slip through the Kalman filter. On the contrary, when all wheels experience excessive slip/slip, the longitudinal acceleration integral is used to estimate the vehicle speed.

When the vehicle is skidding, it is usually in emergency braking or with a large driving force. At this time, the yaw rate and lateral speed are not significant. Therefore, a two-degree-of-freedom vehicle model can be used, and the relationship between the first derivative of the longitudinal speed and the longitudinal acceleration is:

$$\dot{V}_x = a_x + v_y\omega_\gamma \quad (58)$$

Where ω_γ is the yaw rate. By integrating Equation 58,

$$v_x = v_0 + \int (a_x + v_y\omega_\gamma)dt \quad (59)$$

Where, v_0 is initial speed. When switching to the vehicle speed estimation algorithm based on acceleration integration, take the estimated vehicle speed v_x based on the Kalman filter at the last moment as the initial value of acceleration integration.

2.6 Real Vehicle Test Verification

2.6.1 Pylon course Slalom Test

The pylon course slalom and split road test with high

requirements for handling and stability were carried out in the test field, and the test results are as follows.

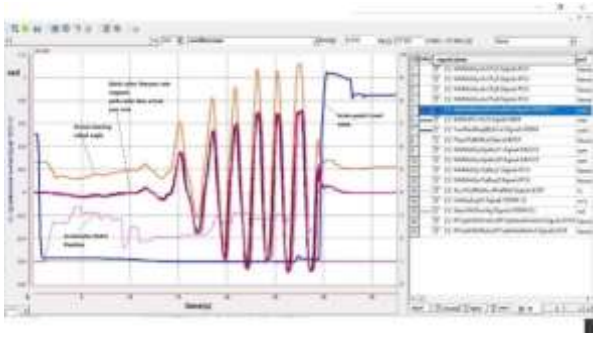

Fig. 14: pylon course slalom test

As can be seen from Figure 15, the steering wheel angle changes between 3.6rad and -3.4rad. As seen in Figure 14, the actual yaw rate (pink line) and the expected yaw rate (black line) follow closely, which means that the control effect is very good to ensure the vehicle's driving stability.

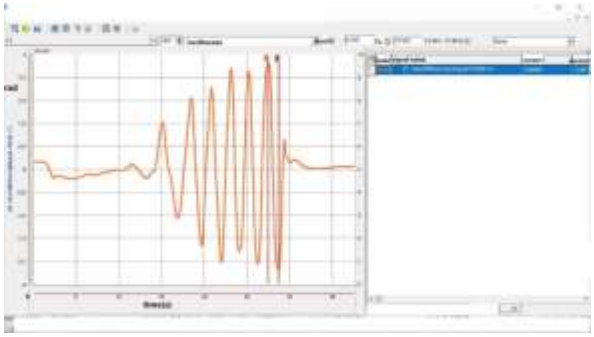

Fig. 15: Steering wheel angle

2.6.2 double-shift Road Test

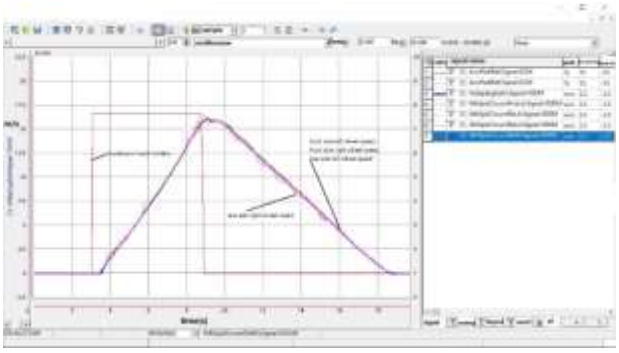

Fig. 16: Double-shift test

The left side of the double-shift road is a high-adhesion asphalt pavement, and the right side is a low-adhesion water-sprayed ceramic pavement. It can be seen that the right rear wheel has a runout, but the overall runout is controlled within an acceptable range, and the other wheels maintain the same speed very well. On the open-circuit surface, the control strategy can still ensure the body's attitude and the vehicle's driving stability. The double-shift test is presented in Figure 16.

2.6.3 Vehicle Jumps from High-Adhesion Road to Low-Adhesion Road

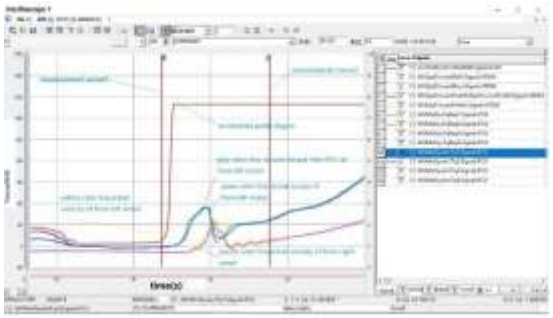

Fig. 17: vehicle is driven from a high-adhesion road to a low-adhesion road

As can be seen from Figure 17, starting from 31.36 second, when the accelerator pedal is pressed at 100% percent the vehicle is driven from a high-adhesion road to a low-adhesion road. From Figure 17, it can be seen that there is a sudden increase in the speed of the front left and front right wheels. This sudden increase is because the distributed controller has yet not detected the change in road adhesion coefficient after the vehicle is driven from a high adhesion road to a low adhesion road. Therefore, the driving force for each wheel driving motor has not been adjusted. Because the driving force of the front left and front right motor is greater than the friction provided by the road to the front left and front right tires, causing each wheel to slip, resulting in a sudden change in the wheel's speed. When the distributed controller has detected the wheels are starting to slip, it quickly invokes the anti-slip control program to adjust the driving torque based on the magnitude of road friction force. As shown in Figure 17, the front left and right wheels' speed increase steadily after being adjusted for 1.4 seconds. The entire process took 1.4 seconds and the control effect was acceptable.

3 Conclusion

A longitudinal speed calculation algorithm is developed by establishing a 7-degree-of-freedom model of a four-wheel drive vehicle equipped with four motors. The vehicle yaw torque is controlled to ensure vehicle driving stability based on the fuzzy control algorithm and using yaw rate and centroid sideslip angle. Based on ECE regulations and the I curve, the optimal strategy of braking energy recovery in the braking process is formulated, which combines stability control and optimal regenerative braking energy feedback control, and comprehensively considers the limited conditions of battery and motor on torque output. The driving or braking torque demand of a four-wheel drive motor is given, which improves the stability of a four-wheel drive vehicle and achieves optimal braking energy recovery. Finally, the actual vehicle test verifies the above strategy's effectiveness.

For this research topic, further in-depth algorithm optimization and more experimental verification are needed. Especially for road surface recognition and speed prediction, conduct more in-depth research.

Another important research direction is the control boundary and control authority division between distributed controllers and ESP/ABS controllers during the braking process, which requires extensive exploration and research.

References :

[1] Zhu Shaopeng, Jiang Xudong , wang yanran, Research on Parallel Braking Control of Distributed Four-wheel-drive Electric Vehicle[J] , Automotive Engineering, 2020, 42(11), p.1506-1512, p.1544. DOI: 10.19562/j.chinasae.qcgc.2020.11.008.

[2] Sun Daxu，Lan Fengchong，Chen Jicqing. A study on the braking energy recovery strategy for a 4WD battery Electric vehicle based on ideal braking force distribution (curve I). Automotive Engineering 2013, 35 (12): p.1057-1061

[3] Huang xueyan, Li yunwu, Liu dexiong, Braking energy recovery control strategy for four-wheel independent drive electric vehicle [J]. Science Technology and Engineering, 2018, 18 (10), p.167-173. DOI:10.3969/j.issn.1671-1815.2018.10.028.

[4] Ji Fenzhu，Du Farong，Zhu Wenbo. Electric vehicle energy economy based on braking intention identification. Journal of Beijing University of Aeronautics and Astronautics，2016; 42 (1), p.21-27. DOI: 10.13700/j.bh.1001-5965.2015.0031.

[5] SHIHONG, SUN, JIN LIN. Direct yaw-moment control for 4WID electric vehicle via finite-time control technique [J]. Nonlinear dynamics, 2017, 88(1), p.239-254. DOI: 10.1007/s11071-016-3240-0.

[6] Nam, K., Fujimoto, H., Hori, Y.: Lateral stability control of in-wheel-motor-driven electric vehicles based on sideslip angle estimation using1ateral tire force sensors. lEEE Trans. Vel. Technol. 61(5), p.1972-l 985, (2012).

[7] Doumiati, M., Victorino, A.C., Charara, A., Lechner, D.: Onboard real-time estimation of vehicle lateral tire-road forces and sideslip angle. IEEE/ASME Trans. Mechatron. 16 (4), p.601-614, (2011).

[8] Fu, C.: Direct yaw moment control for electric vehicles with independent motors. PhD, thesis,RMIT University (2014).

[9] Zhu, B., Chen, Y., Zhao, J., Su, Y.: Design of an integrated vehicle chassis control system with driver behavior identification. Math. Probl. Eng. 2015, l-12 (2015).

[10] Seongjin, Y., Jaewoong, C., Kyongsu, Y. : Coordinated control of hybrid 4wd vehicles for enhanced maneuverability and lateral stability. IEEE Trans. Veh. Technol. 61 (4), p.1946-1950, (2012).

[11] Roshanbin A., Naraghi,M.: Adjustable robustness method for fuzzy logic integrated control of active steer angle and direct yaw

moment. Int. J. Control Autom. 6 (4), 329-3-\46, (20l3).

[12] Kim, C. J., Mian, A.A., Kim, S.H., Back, S.H., Jang, H. B., Jang, J.H., Han, CS.: Performance evaluation of integrated control of direct yaw moment and slip ratio control for electric vehicle with rear in-wheel motors on split-mu road. Int. J. Autom. Technol. 16 (6), p.939-946, (2015).

[13] Qi, Z., Taheri, S., Wang, B., Yu, H.: Estimation of the tire road maximum friction coefficient and slip slope based on a novel tyre model. Vel. Syst. Dyn. 53(4), p.506-525, (2015).

[14] Wang zhenpo, Ding xiaolin, zhang lei. Overview on Key technologies of acceleration slip regulation for four-wheel-independently-actuated electric vehicles [J]. Journal of mechanical engineering, 2019, 55 (12), p.99-120. DOI: 10.3901/JME.2019.12.099.

Appendix

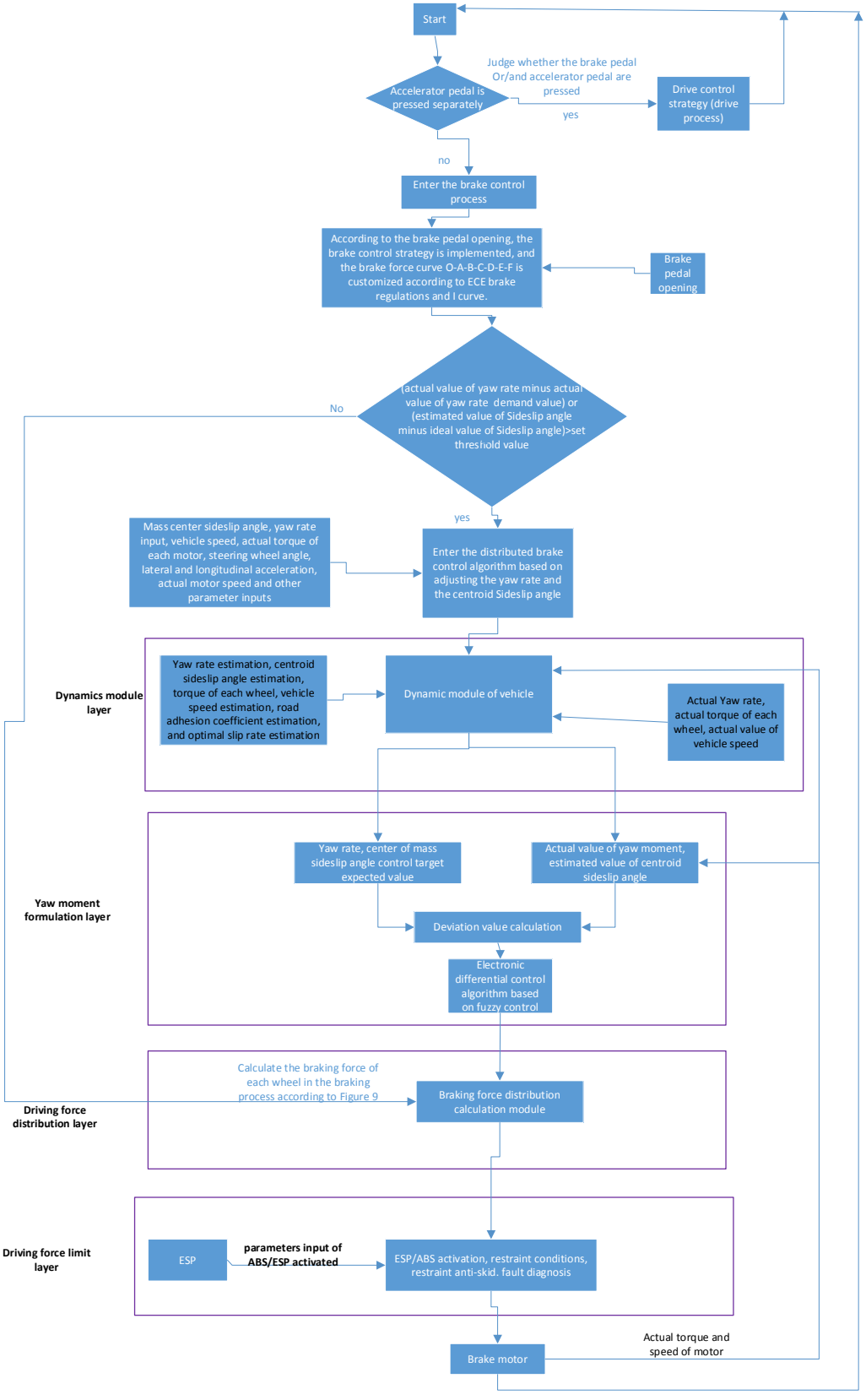

Fig. 4: Flow chart of braking process stability control and optimal braking feedback control

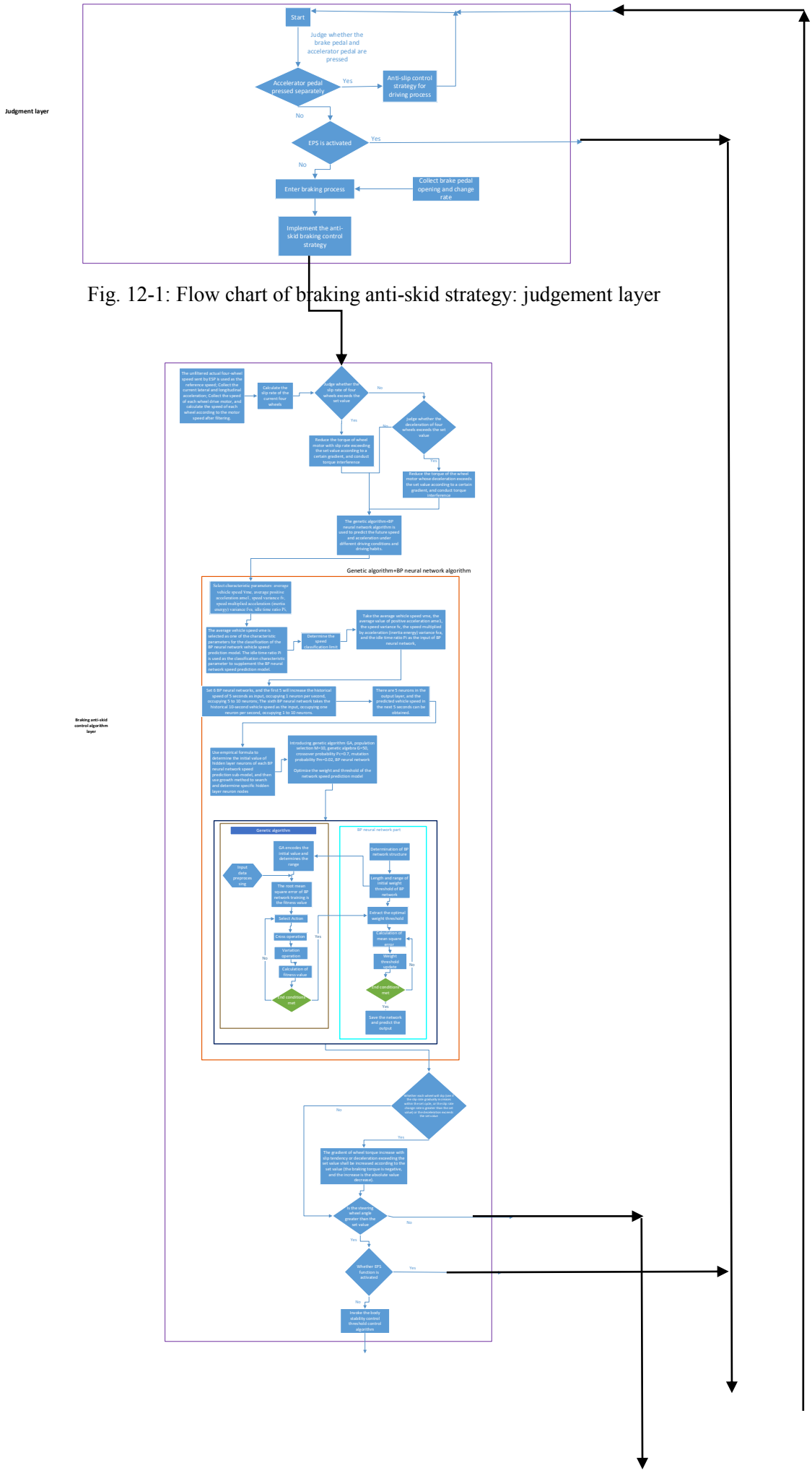

Fig. 12-1: Flow chart of braking anti-skid strategy: judgement layer

Fig. 12-2: Flow chart of braking anti-skid strategy: Braking anti-skid control algorithm layer

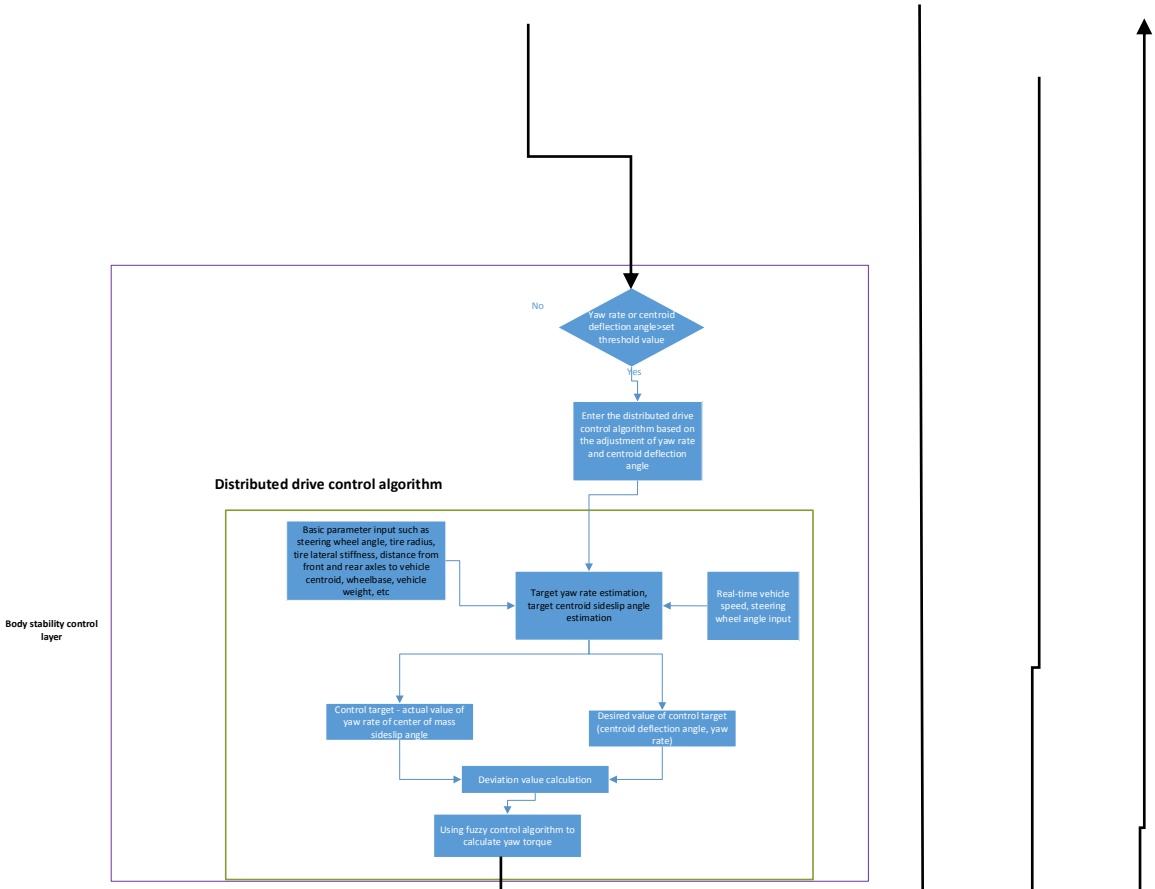

Fig. 12-3: Flow chart of braking anti-skid strategy: Braking anti-skid control algorithm layer

Fig. 12-4: Flow chart of braking anti-skid strategy：Body stability control layer

Table 3. Vehicle speed estimation method

classification	method	Applicable working conditions	merit and demerit	accuracy
Kinematics-based method	Wheel speed method	Good adhesion to road surface, no emergency acceleration/braking conditions	The method is simple and easy to realize, but the adaptability of working conditions could be better, the requirements for wheel speed signal noise are high, and the accuracy could be higher under emergency braking and braking during the acceleration process.	low
	Slope method	Emergency braking condition	Depending on the initial braking speed, many experiments are needed to calculate the acceleration under emergency braking conditions and adapt to different road adhesion conditions.	low
	radar/GPS measurement	Wide application range, not affected by road surface and vehicle status	The signal accuracy is high and easy to obtain, but the signal update frequency is low, and it is easy to be affected by weather and obstacles.	higher
	Wheel speed and acceleration integration method	Any condition，	To some extent, overcome the shortcomings of acceleration and wheel speed signals; However, the accuracy will decline under the limited working condition for a long time.	general
Dynamic-based approach	Kalman filtering	Any condition	Good adaptability to working conditions, and the classical Kalman filtering method is easy to implement in engineering; However, it requires high accuracy of the model and needs real-time acquisition of process noise and observation noise	general
	Observer-based method	Any condition	The estimation accuracy depends on the model accuracy, and the adaptability to the model parameters could be better.	general
Intelligent estimation method	Intelligent estimation method	Specific working conditions (depending on training sample database or fuzzy logic rule base)	It is optional to establish an accurate model of the controlled object, still, the estimation accuracy depends on the training samples, which is challenging to meet the accuracy and real-time requirements of vehicle dynamics control and is difficult to achieve in engineering.	low
fusion method	Multi-information and multi-method fusion	Any condition	The fusion method of multi-sensor and multi-model overcomes the defects of a single method, and has a wide range of applications and high accuracy, but the algorithm logic is complex and requires a high controller.	high

Contribution of Individual Authors to the Creation of a Scientific Article (Ghostwriting Policy)

Yuehang Dong was responsible for all the works of this paper, conceived the presented idea, methodology, implementation, writing, reviewing, and editing, and conducted the experimental testing and verification.

Yuanyuan Yang, Hongjun Zhai, and Changming Zhao were responsible for the project administration.

Sources of Funding for Research Presented in a Scientific Article or Scientific Article Itself

This work is supported through the project funding of Ningbo Geely Automobile Research and Development Co., Ltd.

Conflict of Interest

The authors have no conflict of interest to declare.